Characterisation of Inter-Ply Shear in Uncured Carbon Fibre Prepreg

S. Erland, T. J. Dodwell and R. Butler[1]

Department of Mechanical Engineering, University of Bath, Bath, BA2 7AY, UK.

Abstract

Understanding the inter-ply shear behaviour of uncured carbon fibre prepreg is fundamental to avoiding process-induced defects during manufacturing of large-scale components. Shear tests for AS4/8552 are compared to a one-dimensional viscoelastic-plastic model for inter-ply shear. The paper presents a methodology capable of determining the parameters of temperature, rate and pressure required for minimum resistance to movement of a prepreg. Investigating the joint strength and friction values individually shows that friction increases with temperature, contrary to previous work, and that the new value of joint strength is predominant at lower temperatures. Rate dependent variables are strongly linked to the resin behaviour, confirming the need for a viscoelastic model. Simple application to industrial scenarios is discussed along with more complex process modelling.

Keywords: A. Prepreg; A. Laminates; B. Interface/interphase; C. Analytical modelling.

1. Introduction

Whilst the basic advantages of composite materials are well proven, they are often compromised by high costs, long development time, and poor quality due

[1]Corresponding author: r.butler@bath.ac.uk

to manufacturing defects. This is particularly the case for the complex structures found in large aerospace applications. If laminates are to conform to a surface with curvature during forming or consolidation, plies within a laminate must shear relative to one another. If plies are prevented from shearing the process becomes susceptible to generating a host of manufacturing induced defects including ply wrinkling [1, 2, 3, 4] (e.g. Fig. 1), part distortion [5, 6] and poor consolidation [7]. To limit the formation of such defects, the characterisation of shear properties of materials is vital to not only determine optimal shear conditions for manufacturability, but to provide input parameters for process simulations [3] and manufacturing design methods [8].

A number of studies [9, 10] have investigated inter-ply slip properties of uncured carbon fibre pre-preg. In each case the shear rheology is characterised by a temperature dependent coefficient of friction. Using an inter-ply slip-rig similar to that used in this contribution (Section 3), the studies showed significant variability between different generations of carbon fibre pre-preg [10]. However, in each case, inter-ply friction displayed a convex dependence on temperature, attaining a minimum at an intermediate manufacturing temperature. The work attributed the initial decrease in friction to hydrodynamic lubrication of the inter-ply region as the resin viscosity decreases with temperature, whilst the subsequent increase was due to intensified intermingling of fibres at higher temperatures. Further experimental work has therefore focused on determining surface roughness measures [10] and understanding matrix distribution at different stages of the various processes, whilst using Stribeck theory [9, 11] to determine different regimes of hydrodynamic frictional behaviour.

The use of a frictional model suggests that the layered structure is infinitely stiff in shear, and that any deformation occurs in the form of slip at the interface above a critical value of stress. Stress/strain traces from the work of Larberg et

al. [10] suggest this to be a simplification, noting the presence of some pre-yield stiffness before a post-yield response after a gradual transition. For forming processes in which shear strains are relatively small (e.g. consolidation over a corner radius, Section 5.7.) the purely frictional model can significantly overestimate the shear stresses. Whilst these general observations are supported by this paper, we extend the characterisation of inter-ply shear behaviour developed in [10] to account for a number of key dependencies not previously investigated; primarily the strong rate dependency, arising from the viscoelastic contribution of the resin.

In Section 2 we introduce a one-dimensional viscoelastic-plastic model which captures the behaviour observed in the literature, with Section 3 describing the experimental method developed to validate it. This model, parameterised by the experimental data (Section 4), provides simple metrics by which to compare through-thickness shear properties (Section 5), for different materials and manufacturing conditions. We also consider application to two different manufacturing scenarios, forming and consolidation over corner a radius (Section 5.7). Whilst previous work suggests optimum manufacturing conditions are independent of manufacturing process, the parameterised model presented here suggests process dependent conditions for optimal manufacturability. The paper concludes with a summary of the key findings, and possible future avenues of research.

2. One dimensional viscoelasto-plastic model for inter-ply shear

Firstly, a one-dimensional viscoelasto-plastic model for inter-ply shear of uncured laminates is introduced, before the process by which the modelling parameters can be constructed from the experiments is described.

The pre-yield behaviour is decomposed into rate dependent and independent

parts. A constitutive law with these characteristics, is given by the relationship

$$\tau = \left(G + \eta \frac{d\gamma}{dt} \right) \gamma = K\gamma \tag{1}$$

where G is the rate independent elastic shear stiffness, η the coefficient of viscosity and $d\gamma/dt$ the strain rate. The parameter K denotes the overall initial rate dependent shear stiffness. Shear strains encountered in both industrial forming processes and the experimental setup can be large (i.e. $\gamma > 0.5$), therefore 'true' strain measures are considered. If $u(t) = Rt$ is the displacement for some constant displacement rate R, h is the through thickness dimension (where for the material used, individual ply thickness $h/2 = 0.25$mm) it follows that

$$\gamma = \ln\left(1 + \frac{Rt}{h}\right) \quad \text{and} \quad \frac{d\gamma}{dt} = \frac{R}{h + Rt}. \tag{2}$$

For small shear strains such as those seen in the initial response, i.e. γ <0.15, t is small and it can be assumed that $d\gamma/dt \simeq R/h$.

It is important to select an appropriate thickness value. Considering the structure of a laminate as being a series of thick stiff fibrous layers and thin weak resin layers, it seems logical to assume that deformation will localise to the resin layer. Observing the formation of the model however, we can see that changing the thickness will result in a simple ratio change, so long as the same thickness is used throughout. For the purposes of this paper, in which tests are conducted for two plies and one deformable interface, we take h to be twice the ply thickness such that the results can be more readily scaled to laminate deformation. This approximation is discussed in more detail in Section 5.

The onset of inter-ply slip is defined by a Mohr-Coulomb yield criterion

$$\tau_c = \mu\sigma_n + j \tag{3}$$

such that μ is the coefficient of friction, σ_n is the normal stress and j a measure of joint strength. Joint strength initially appears similar in concept to tack, however the parameter presented here specifically describes the shear joint strength, whereas tack relates to the tensile joint strength.

Supposing yield has occurred (i.e. $\tau \geq \tau_c$), an additional strain increment is applied $\Delta\gamma$. This strain increment can be decomposed into viscoelastic ($\Delta\gamma_{ve}$) and plastic ($\Delta\gamma_p$) contributions, so that $\Delta\gamma = \Delta\gamma_{ve} + \Delta\gamma_p$. It follows that

$$\Delta\tau = K\Delta\gamma_{ve} = K(\Delta\gamma - \Delta\gamma_p). \tag{4}$$

The hardening rule, to account for the post yield stiffness, is then defined by

$$\Delta\tau = H\Delta\gamma_p, \tag{5}$$

where H is the strain-hardening parameter. Equating Eqs. (4) and (5) it follows $H\Delta\gamma_p = K(\Delta\gamma - \Delta\gamma_p)$ so that $\Delta\gamma_p = \frac{K}{H+K}\Delta\gamma$. Therefore the post yield response is given by the expression

$$\Delta\tau = G_t\Delta\gamma = K\left(1 - \frac{K}{K+H}\right)\Delta\gamma \tag{6}$$

where G_t is termed the consistent tangent stiffness. Rearranging for the hardening parameter gives the expression

$$H = \frac{KG_t}{K - G_t}. \tag{7}$$

This model gives an idealised bi-linear response, as shown in the stress-strain plot Fig. 11. The modelling parameters can be approximated from the experimental stress-strain data by first constructing two lines of best fit from the pre and post yield load paths. The gradients of which are approximations

to K and G_t (Fig. 11), whilst their intercept gives the critical shear stress τ_c.

First, to determine G and η, the pre-yield gradient K is calculated for increasing strain rates R, as shown in Fig. 2. It follows from Eq. (1), that the rate independent parameter G is given by the y-intercept, whilst η can be fitted in the least square sense, in this paper using Matlab's inbuilt function `cftool`. Secondly, the coefficient of friction μ and joint strength j are determined by calculating τ_c over a range of confining pressures σ_n. Figure 3 shows a typical plot, fitting a straight line to the data, the y-intercept gives the joint strength j, whilst the gradient is the coefficient of friction μ. Finally the hardening parameter H is determined by applying Eq. (7) using gradients K and G_t.

3. Experimental procedure, material and sample preparation

Figure 4 (Left), shows a schematic of the test rig which consisted of two independent components. Firstly, a lock-able hinged array connected to an Instron load cell at (i), consisted of a pneumatic cylinder (ii) which pulled together two plates (area, A = 50×50 mm^2) wrapped in a single layer of carbon fibre prepreg (iii). These plates clamped either side of a central plate (area, A = 100×150 mm^2)(iv), also wrapped in a layer of carbon fibre prepreg, which was fixed to the bottom mounting of an Instron testing machine (v). The carbon fibre was wrapped and clamped in such a way as to prevent movement of the ply relative to the plate surface. The rig was mounted within an environmental chamber, allowing the temperature of test to be controlled. The test procedure was as follows: (1) test temperature was achieved in the environment chamber (2) the pressure in the pneumatic cylinder was controlled to generate a normal clamping stress σ_n between the side and central plates (3) the Instron pulled the upper part of the rig at a constant rate $R = du/dt$, whilst the load cell recorded the force F. All experiments were carried out using AS4/8552, wrapped around

each plate so that the fibres were oriented vertically (i.e in the direction of loading, referred to as 0°). This material was chosen as it is effectively the genesis material for a series of prepregs commonly used in the aerospace industry. Note that although it was decided to focus on a single material, primarily due to the quantity of tests being carried out, the modelling above can be applied to any thermoset prepreg. Tests were conducted at a range of rates R, temperatures and confining pressures σ_n. Each test was conducted three times to ensure repeatability of results. The set of tests carried out are summarised in the test matrix, Table 1.

3.1. Rig calibration and measures to minimises sources of variability

Before carrying out these tests it was necessary to calibrate the rig for a material with a known coefficient of friction. A number of tests were carried out using PTFE instead of CFRP; giving an average value of $\mu = 0.096$, which was within the documented range of 0.05-0.10 [12]. The following operational caveats were noted:

Side plates: By rigging extensometers between the side and main plates it was possible to monitor any potential discrepancies between the crosshead displacement and that of each plate. Over the course of several experiments it was proven that differential movement did not occur to any noticable extent. A similar technique was also employed to ensure that the side plates did not rotate upon being loaded.

Controlling constant confining pressure: It was reasoned that the load applied by the pressure cylinder could be monitored by observing the pressure gauge on the air feed. Any fluctuations in this pressure would indicated a change in lateral loading. Due to the relatively low loads required to slip the interfaces it was also necessary to use a sufficiently accurate load cell with a maximum capacity of 1kN.

Controlling temperature: Temperature was measured by means of a thermocouple attached to the edge of one of the side plates. As the plates themselves are small and made of mild steel they have a fairly high coefficient of thermal conductivity, therefore it was safe to assume that the temperature at the middle of the plate would not differ significantly from that at the edge, and was well within the +/- 5°C tolerance expected by industry in the manufacturing stages.

Consistency of sample: To ensure minimal out time from the freezer, each sample was defrosted for 20 minutes and prepared immediately before testing from larger cut sheets to avoid repeatedly defrosting the entire role of material. During the test regime the target temperature was reached and held for 5 minutes before pressure was applied to ensure the samples were fully heated. Unfortunately, it was not possible to measure the expected change in ply thickness during the test. As such, the thickness value used in Section 2 was assumed to remain constant.

4. Results

Figures 5 and 6 display stress/strain traces for tests conducted at a variety of temperatures, pressures and rates. The traces show the same general behaviour, with an initial stiff response changing to a less stiff response after a gradual yield.

Figure 7 shows how the joint strength j and coefficient of friction μ change with increasing temperature. Joint strength (Fig. 7 (Left)), strictly decreases with increasing temperature. However, the coefficient of friction strictly increases with temperature, Fig. 7 (Right). In Table 2 all values of j and μ with associated regression coefficients are given. The variation of critical shear stress τ_c against temperature is plotted in Fig. 8 with associated error bars, reaching a minimum at $90°C$.

The rate dependent data provides parameters for the viscoelastic model, see

Table 3. The plots of G and η, shown in Fig. 9, show that both values strictly decrease with temperature. However, strain hardening parameter H against temperature displays a peaked response, reaching an apparent maximum at approximately 60°C (Fig. 10).

Due to the manner in which modelling parameters are derived, there is a mix between error bars and regression coefficients. Values which were drawn directly from the stress/strain traces, i.e. K and τ_c, are shown with error bars generated from repeat tests. The remaining modelling parameters are gathered from fitting data to these parameters, as such they are displayed with regression coefficients as they were not repeated. Typically, the error bars were relatively small, with an average error of 4-6% for K values and slightly more error (10-12%) for τ_c values as a result of τ_c being dependent upon two testing variables.

5. Discussion

5.1. Stress/strain traces

The stress/strain traces of Figs. 5 and 6 obtained for variable temperature, pressure and rate show a similar response to those displayed by Larberg et al. [10], whereby each plot has two distinct regions. The first region, characterized by an initial stiffness, can be attributed to the shear behaviour of the two plies at small strains, before the interface yields. This is followed by a second region at a reduced stiffness. Figure 5 (Left) shows the influence of temperature on these stress/strain traces. Increasing the temperature clearly reduces the initial stiffness and the yield point of the material, confirming the influence of the uncured resin on this initial response. Figure 5 (Right) shows the pressure dependency of the yield point, confirming the presence of some frictional behaviour. Interestingly, the initial stiffness is not affected whereas the post yield response clearly becomes stiffer with increased pressure. This suggests that the

initial response is governed by the viscous uncured resin, whereas the yield and the post yield response are more frictional. The final trace, Fig. 6, further confirms this, showing a considerable rate dependency in the initial load response, thereby confirming the viscoelastic contribution of the resin. In order to better investigate the influence of temperature, pressure and rate we can now consider the new paramters derived in Section 2.

The bi-linear model developed in Section 2 is applied to a standard stress/strain trace in Fig. 11. From similar stress/strain traces, Larberg et al. [10], derive a single coefficient of friction. Such a simple model is therefore not capable of capturing the full shear behaviour observed. Models considering the material to be elastic will also misrepresent uncured behaviour [13].

5.2. Interply yield

Figure 8 is similar to results presented by Larberg et al. [10] and Dodwell et al. [3], who both plotted coefficient of friction at yield against temperature. Figure 8 differs in that τ_c is a combination of the effects of friction, μ, and the new parameter, joint strength j. The plot shows an initial decrease in τ_c as temperature increases, reaching a minimum at $90°C$, after which τ_c increases with temperature. Dividing the shear into two separate mechanisms, as shown in Fig. 7, gives a better insight into the combined mechanics which contribute to τ_c. Comparing the values of j in Fig. 7 (Left) with the values of τ_c in Fig. 8 we see that the parameter j dominates at lower temperatures suggesting that pre-yield behaviour plays a more significant role at low temperatures. From Fig. 8 the minimum reached at 90°C marks the point at which slip becomes the dominant mechanism. The behaviour of μ is particularly important. Previous work presented μ as a value with behaviour similar to the value of τ_c in this work, suggesting that μ is initially high at low temperature then falls to a minimum value before increasing again with temperature. This new model shows μ to be

minimal at low temperatures then strictly increasing as temperature increases.

A possible explanation is that at low temperatures the fibres within each ply are separated by a thick layer of resin, formed from the resin rich zones present on the surface of each ply. This reduces the inter-ply friction between fibres and the response is dominated by the shearing of the resin rich region. As temperature increases the resin layer is initially maintained, with the softened response being due to the lower shear modulus of the material at elevated temperature. As the temperature rises further the resin flows into the dry core of the plies [14], increasing fibre-fibre contact between adjacent plies. At this stage the increased level of fibre-fibre contact means that the results are almost purely frictional. This is illustrated by Fig. 12 (Left), which shows a cross section of unconsolidated AS4/8552 prepreg and Fig. 12 (Right) showing a cross-section of the same material after it has been heated to 80°C and had a normal stress of 100kPa applied.

Figure 12 (Left) shows a large amount of resin towards the surface of the ply, with a very noticeable dry core. By contrast, in Fig. 12 (Right) the resin appears to be distributed fairly uniformly following consolidation at temperature, with more fibres on the outer edge. There is also a considerable reduction in ply thickness as the resin has redistributed. This supports the hypothesis that low temperature interaction will be dominated by the resin layer, whereas high temperature interactions will be increasingly influenced by fibre-fibre contact.

5.3. Viscoelastic parameters

By plotting K against $d\gamma/dt$ (Fig. 2) we can determine the rate independent elastic modulus G from the y-intersect. From Fig. 9 (Left) it is immediately apparent that this value is very small when compared to the material response at even the slowest rate of deformation, confirming the importance of modelling the initial response as a combined visco-elastic material.

Figure 9 shows the variation of the rate independent part of K with temperature. Figure 9 (Right) displays η values calculated via Eq. (1) and how this value is also clearly influenced by temperature. Compared against Hexcel data sheets η is significantly higher than viscosity values quoted for pure 8552 resin at similar temperatures [15]. This is thought to be due to the resin being mixed with fibres. Whilst there is a layer of pure resin in the middle of the laminate, it can be seen in Fig. 13 that this layer is not uniform in any sense. As such, the fibres will contribute to the shear modulus of this region, and the viscosity. The stiffer the resin, be it due to rate or temperature, the more stress will be transferred to the fibres.

5.4. Post yield hardening

Figure 11 displays the stress/strain trace for a test conducted at 70°C with a normal pressure of 75kPa. The initial response discussed earlier can be observed as the steep initial gradient, before the yield point leads into the region of post-yield hardening. The phenomenon of this post yield stiffness or hardness can also be observed in the stress/strain traces presented by Larberg *et al.* [10]. Confidence in the rig function has been obtained by conducting a test whereby PTFE was wrapped around the plates rather than CFRP, resulting in a zero stiffness post yield response as expected of a frictional material, with a coefficient of friction of 0.096 which falls within the expected range for this material. This confirms that the post yield hardening is due to the material and not the test setup. Figure 10 shows the hardening parameter H peaks at 70°C before falling rapidly as temperature increases. This hardening effect may be due to the slow rate at which the tests are conducted. This could result in the liquid resin reforming the joint post yield, preventing transition to pure slip. At low temperatures the resin is too viscous to allow the joint to reform, however as the temperature increases the resin becomes sufficiently fluid to allow reforming of

the joint. By 90°C the resin has become so fluid that it has almost fully flowed into the fibre core. As such, little resin remains at the ply-ply interface and we instead see an almost frictional response, with very little hardening. Fibre pullout tests conducted by Dodwell et al. [3] employed a much higher rate R of 1mm/min, and the stress/strain traces obtained showed little or no evidence of post yield hardening, suggesting the increased rate was sufficient to prevent reforming of the interface, either through the effective stiffening of the resin due to rate, or simply due to the speed of deformation. This appears to be confirmed when applying Eq. (7) upon which it can be seen that the post yield modulus, G_t decreases as rate increases.

5.5. Inter-ply slip versus laminate shear

The discussion and results presented suggest that inter-slip behaviour is the result of localised mechanisms at the ply interface. However, the shear strains and strain rates presented are all calculated relative to ply thicknesses, rather than the thickness of the interface. The principal reasoning behind this is that the characterisation has been designed with laminate behaviour in mind (see Section 5.7). Laminate shear parallel to the layering can be modelled as a set of two shear springs in series; a soft spring for the interface and a stiffer spring for the fibrous ply. Shear modulus here is denoted as S, where S is equivalent to K and G_t of Eqs. (1)and (7). From [16] we see that $h_{fib.} \simeq 16 h_{int.}$ and $S_{fib.} \simeq 1000 S_{int.}$, thus

$$\frac{\bar{h}}{S} = \frac{h_{int.}}{S_{int.}} + \frac{h_{fib.}}{S_{fib.}} \simeq \frac{h_{int.}}{S_{int.}} \left(1 + \frac{16}{1000}\right) \simeq \frac{h_{int}}{S_{int}}. \tag{8}$$

where $\bar{h} = h_{int.} + h_{fib.}$. From this we see that the shear stiffness of a laminate parallel to the layering is dominated by the weak interface whilst the contribution to laminate shear from the fibrous region is negligible, as such $S = S_{int.}\bar{h}/h_{int.}$ The laminate shear stiffness S is therefore an approximation

of the shear behaviour of the ply as a result of localised shear or slip at the interface between the constituent layers. Considering shear behaviour on a ply level, the strain can be simply changed based on the h ratio from [16], changing the strain axis on the results without affecting the behavioural pattern. For this work laminate shear stiffnesses are considered since these are most relevant for the laminate-scale consolidation and forming applications considered in Section 5.7

5.6. Discussion of potential errors and model limitations

With the careful application of certain caveats as discussed in Section 2, it was possible to achieve a very high level of repeatability during testing. There are however some limitations with this test rig. As the experimental set-up was contrived to investigate a specific material function, i.e. inter-ply slip, certain inconsistencies in mechanism exist when compared to a real application. A particular limitation with the model is that it is one dimensional with shear occuring on a single plane. In reality the shear is also through thickness, and as discussed is influenced by the irregular geometry of the interface, making it two dimensional. As such accuracy suffers and certain behavioural aspects are overlooked. The model also assumes an initial elastic behaviour, suggesting that at small strains the deformation will reduce to zero when load is removed, which does not seem feasible due to the viscous nature of the resin being dominant at these strain levels [17]. Whilst this model is a good starting point it is clear that further investigation is needed into these areas.

5.7. Optimum forming parameters for process induced shear strains

By understanding the geometry of the part and forming process employed it is possible to calculate the shear strain required for the part to conform to the required geometry; minimising the likelihood of manufacturing defects (see for

example the out-of-plane wrinkles shown in Fig. 1). If we consider two different forming approaches we can understand the difference in shear strain required for defect free forming. First we consider a debulk scenario (Fig. 14) (Left), such as might occur after deposition of plies around a radius.

The total slip at the free edge can be calculated as the difference between the outer arc length before and after debulk. The pre-debulk arclength $s_{\text{pre}} = (r+\frac{1}{2}(Nh))\theta$, where r is tool radius, N is number of plies, θ is tool angle and $h/2$ is ply thickness. The post-debulk arc length $s_{\text{post}} = \theta(r-\frac{1}{2}((1-\alpha)Nh))$, where α is the percentage consolidation. Therefore for the consolidation scenario, the required shear strain is

$$\gamma_{\text{cons.}} = \ln\left(1+\frac{s_{\text{pre}}-s_{\text{post}}}{\frac{1}{2}(Nh)}\right) = \ln\left((1-\alpha)\theta\right). \tag{9}$$

Figure 14 (Right) relates to a drape forming scenario in which a laminte is laid flat then formed to a geometric tool. For this example the inter-ply slip is the difference in length between the arc length at the outer radius $s_{\text{post}} = \theta(r+\frac{1}{2}(Nh))$ and the length of the laminate $s_{\text{pre}} = \theta r$. Thus

$$\gamma_{\text{form}} = \ln\left(1+\frac{s_{\text{post}}-s_{\text{pre}}}{\frac{1}{2}(Nh)}\right) = \ln\left(1+\theta\right) \tag{10}$$

Shear strain generated is thus dependent on the angle of the corner radius θ, and for the consolidation case the level of consolidation. In both cases the shear strain increases incrementally as we move away from the axis of symmetry, reaching a maximum at the free edge. Thus if $\theta = \pi/2$ and consolidation $\alpha = 12\%$ [7, 3], the corner consolidation example generates a maximum shear strain of $\gamma_{\text{cons.}} = 0.32$, whilst the drape forming scenario requires a much greater shear strain of $\gamma_{\text{form}} = 0.94$.

By consulting the material specific stress/strain traces it is possible to deter-

mine which combination of forming parameters will minimise the shear stress to achieve that particular shear strain. In Fig. 14 (Left) the shear strain required to consolidate the part is 0.32. At low strains the key variables are the initial stiffness, K, and the critical shear stress, τ_c.

The scenario displayed in Fig. 14 (Right) induces a much higher shear strain of 0.94. In this instance we are looking to minimise both H and τ_c. High temperature is still desirable and results appear to suggest the forming process might be conducted at a high rate of deformation, contrary to both intuition, and results presented in [17]. It is important to note that this is assuming inter-ply slip is the only factor affecting wrinkle formation. However, this data is drawn from tests deliberatly designed to isolate the shear behaviour on flat plates. Whilst reducing resistance to slip reduces the end load generated by shear, it also causes the plies to act individually, rather than as a laminate, increasing vulnerabilty to wrinkling via end load generated from other sources.

5.8. Application to laminate modelling

The work presented works well when considering the movement of one ply relative to another. However, the package this forms is not immediately suitable for upscaling into a many-layered laminate, as it effectively consists of one resin interface layer between two full fibrous layers, as the resin at the ply to tool interface is disregarded due to the manner in which the sample is clamped. The optimum package for upscaling would consist of a single full resin inteface between two fibrous layers of half thickness. However, if we were to use this value of h to determine the experimental shear strains, we would need to account for the reduction in stiffness due to the omitted fibrous region by reducing the measured deformation proportionately. This would require a much more comprehensive understanding of the individual contributions of the fibrous and resin layers to the overall stiffness. By adopting the two ply package used in this

paper we are able to propose a conservative estimate of the optimum forming parameters, as the test package is actually thicker than the repeatable package, resulting in a lower prediction of shear strain for a given value of applied stress than would actually occur.

6. Concluding remarks and future work

The focused test program has allowed a thorough investigation of the AS4/8552 material, giving a clear insight into how the manipulation of temperature, pressure and rate can influence the behaviour of uncured prepreg. A new model has been presented that combines elastic and plastic behaviour in order to characterise the through thickness shear response of uncured composite pre-preg. This model avoids the overestimation of yield stress acquired from a purely frictional (plastic) model, and avoids the underestimation presented by a purely elastic model. The combination of these two behaviours allows for increased accuracy when considering shear strain levels encountered during the forming of production parts. The model is a first step however as the yield point predicted and subsequent change in gradient of the stress/strain trace is instant, whereas experimental stress/strain traces show a more gradual transition. As a result, the model slightly overestimates the yield stress, however it is a significant improvement over the estimation from a purely frictional model.

The test methodology has proven itself capable of predicting the parameters required for minimum resistance to ply mobility, with temperature having the largest impact. For AS4/8552 prepreg minimum resistance is at a temperature of 90°C, for other materials it is expected that a similar minimum resistance point will also be primarily temperature dependent due to the nature of uncured resin. Other parameters can be manipulated to further improve formability depending on the manufacturing process used. Certain applications require the

use of pressure, such as the example discussed in Section 5.7, where the aim is to achieve maximum consolidation through the use of pressure. As such, the pressure effectively both drives and restricts the slip. It therefore becomes necessary to balance the pressure required to consolidate the part against the pressure required to allow plies to slip within the laminate. Using the results provided here it is possible to offset the negative influence of the high pressure required by choosing an optimum temperature and rate.

Material parameters derived from this technique have already been used to accurately predict wrinkle formation in a corner consolidation model derived by Dodwell et al. [3, 4], with results comparing favourably with data gathered from industry.

Acknowledgements

The authors would like to acknowledge GKN Aerospace for supporting this work. In particular we are grateful to Ian Lang and Dr. Richard Newley for many useful discussions, and for the supply of material. Richard Butler holds a Royal Academy of Engineering/GKN Aerospace Research Chair in Composites Analysis.

References

[1] J. S. Lightfoot, M. R. Wisnom and K. Potter. A new mechanism for the formation of ply wrinkles due to shear between plies. Composites, Part A 2013. 49:139-147.

[2] P. Hallander, M. Akermo, C. Mattei, M. Petersson and T. Nyman. An experimental study of mechanisms behind wrinkle development during forming of composite laminates. Composites Part A 2013. 50:54-64.

[3] T.J. Dodwell, R.Butler, and G. W. Hunt. Out-of-plane ply wrinkling defect during consolidation over an external radius. Composites Science and Technology 2014. 105:151-159.

[4] T. J. Dodwell. Internal buckling instabilities in layered media. Philosophical Magazine - Instabilities Across the Scales IV. In press 2015. DOI:10.1080/14786435.2015.1034221

[5] N. Ersoy, T. Garstka, K. Potter, M. R. Wisnom, D. Porter and G. Stringer. Modelling the spring-in phenomenon in curved parts made of a thermosetting composite. Composites Part A 2010. 41:410-418.

[6] A. R. A. Arafath, R. Vaziri and A. Poursartip. Closed-form solution for process-induced stresses and deformation of a composite part cured on a solid tool: part I - flat geometries. Composites Part A 2008. 39:1106-1117.

[7] T. A. Fletcher, R. Butler and T. J. Dodwell. Anti-symmetric laminates for improved consolidation and reduced warp of tapered C-sections. Advanced Manufacturing: Polymer and Composites Science. Accepted 2015.

[8] P. Boisse, N. Hamila, E. Vidal-Salle and F. Dumont. Simulation of wrinkling during textile composite reinforcement forming. Influence of tensil, in-plane shear and bending stiffnesses. Composites Science and Technology 2011. 71(5):683.

[9] N. Ersoy, K. Potter, M. R. Wisnom and M.J. Clegg. An experimental method to study the frictional processes during composites manufacturing. Composites Part A 2005. 36A:1536-1544.

[10] Y. R. Larberg and M. Akermo. On the interply friction of different generations of carbon/epoxy prepreg system. Composites: Part A 2011. 42:1067-1074.

[11] G. W. Stachowiak and A. W. Batchelor Engineering Tribology 2000. Butterwoth-Heinemann.

[12] W. Wieleba. The statistical correlation of the cefficient of friction and wear rate of PTFE composites with steel counterface roughness and hardness. Wear 2002. 252 9-10:719-719.

[13] A. Johnston, R. Vaziri and A. Poursartip. A plane strain model for process-induced deformation of laminated composite structures. Journal of Composite Materials 2000. 35:1435-1469.

[14] G. S. Springer. Resin flow during the cure of fiber reinforced composites. Journal of Composite Materials 1982. 16:400-410.

[15] P. Hubert, A. Johnston, A. Poursartip and K. Nelson. Cure kinetics and viscosity models for hexcel 8552 epoxy resin. International SAMPE symposium and exhibition 2014. 2341-2354.

[16] T. J. Dodwell, S. Erland and R. Butler. A Cosserat continuum model for uncured composite laminates with applications to ply wrinkle formation. 20^{th} International Conference on Composite Materials, Copenhagen, July 2015.

[17] K. Potter. In-plane and out-of-plane deformation properties of unidirectional preimpregnated reinforcement. Composites Part A 2002. 33:1469-1477.

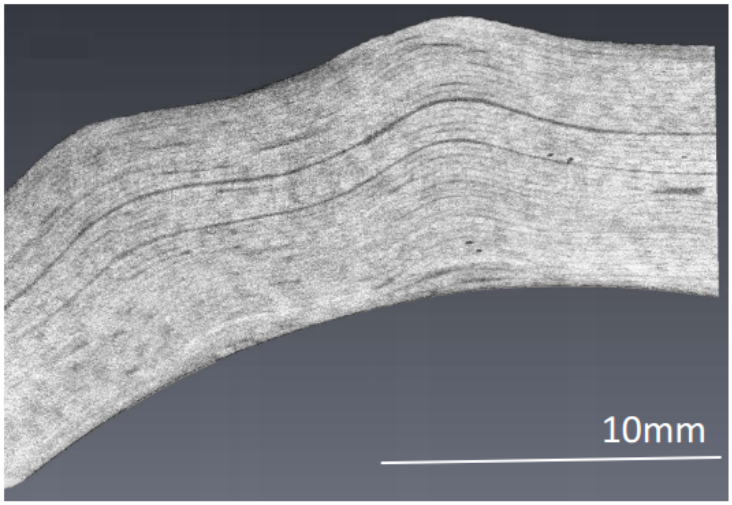

Figure 1: CT image of a typical wrinkle defect within a corner, arising due to the inability of layers to slip over one another [3].

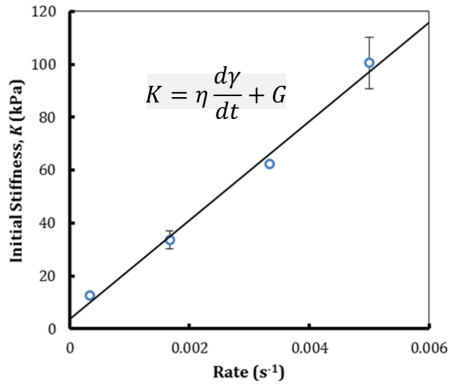

Figure 2: Plot of K against $d\gamma/dt$ for a fixed temperature $T = 70°$ at a fixed pressure $\sigma_n = 75$kPa

.

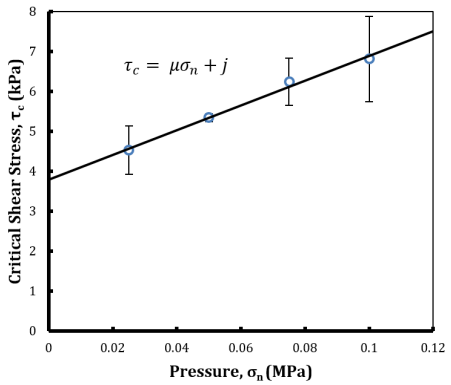

Figure 3: Plot of critical yield stress τ_c against normal stress σ_n for a fixed temperature $T = 40°\text{C}$ and strain rate $d\gamma/dt = 3.33 \times 10^{-3} s^{-1}$.

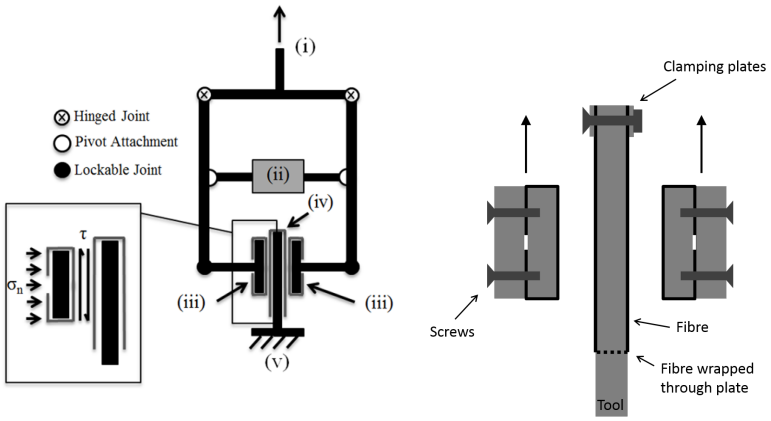

Figure 4: (Left) Schematic of interply test rig in which the two individual parts move apart at constant rate du/dt and the required force is recorded. (Right) Detail of the fibre-plate clamping, with arrows denoting the direction of travel of the side plates. The dashed line on the centre plate indicates where the ply is passed through a gap in the tool so that it is effectively clamping itself.

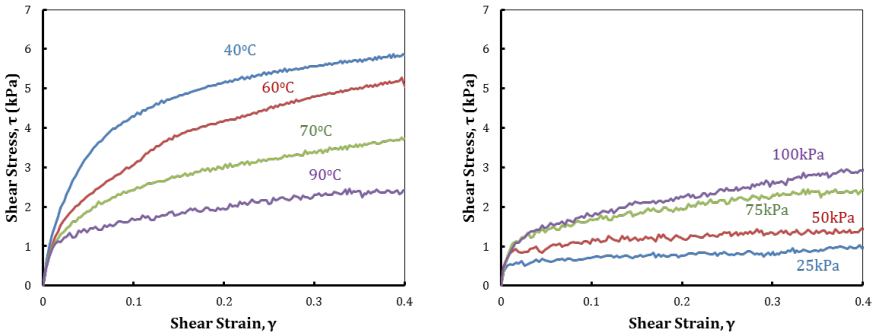

Figure 5: (Left) Shear stress τ against shear strain γ for varying temperature. The data was generated at a fixed rate $d\gamma/dt = 3.33e^{-3}s^{-1}$ and pressure $\sigma_n = 75kPa$.(Right) Shear stress τ against shear strain γ for varying pressure, σ_n. The data was generated at a fixed rate $d\gamma/dt = 3.33e^{-3}s^{-1}$ and a temperature of $90°C$.

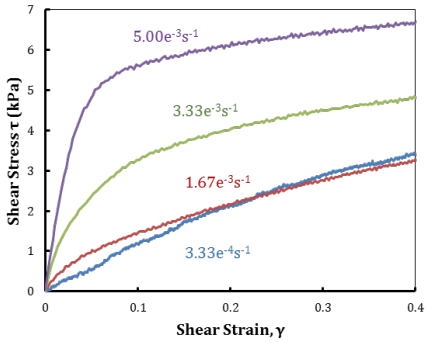

Figure 6: Shear stress τ against shear strain γ for varying strain rate, $d\gamma/dt$. The data was generated at a fixed temperature of $70°C$ and pressure $\sigma_n = 75kPa$.

Rate R **(mm min^{-1})**	**Pressure** σ_n **(kPa)**	**Temperature** $(°C)$						
		40	**50**	**60**	**70**	**80**	**90**	**100**
0.01	**75**	-	×	×	×	-	×	-
0.05	**75**	-	×	×	×	-	×	-
0.1	**25**	×	-	×	-	×	×	-
0.1	**50**	×	-	×	-	×	×	-
0.1	**75**	×	×	×	×	×	×	×
0.1	**100**	×	-	×	-	×	×	-
0.15	**75**	-	×	×	×	-	×	-

Table 1: Experimental matrix for AS4/8552. Each × represents a set of at least 3 repeated experiments

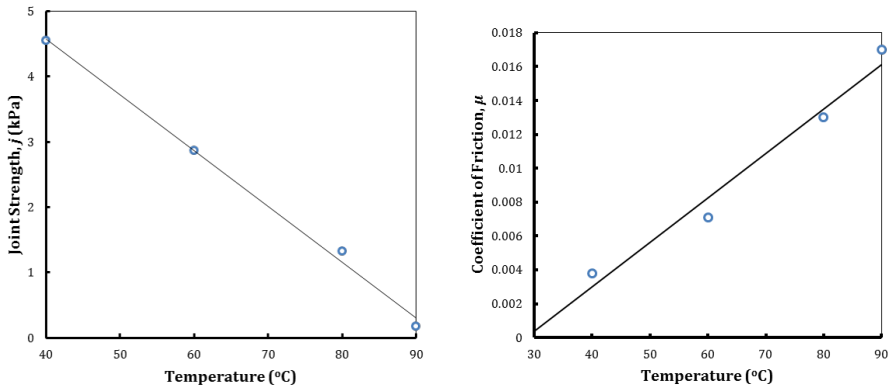

Figure 7: (Left) Joint strength j against temperature. (Right) Coefficient of friction μ against temperature. The data for both plots was generated at a fixed rate $d\gamma/dt = 3.33e^{-3}s^{-1}$.

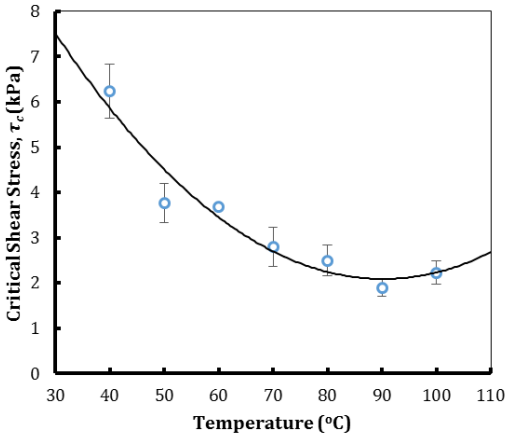

Figure 8: Critical shear stress τ_c against temperature, for a strain rate $d\gamma/dt$=$3.33e^{-3}s^{-1}$.

	40°C		**60°C**		**80°C**		**90°C**	
	Value	R^2	Value	R^2	Value	R^2	Value	R^2
j **(kPa)**	4.55	0.960	2.86	0.915	1.33	0.978	0.180	0.979
μ	0.00381		0.00709		0.0135		0.0173	

Table 2: Experimentally derived regression coefficients for j and μ at a fixed rate $d\gamma/dt = 3.33e^{-3}s^{-1}$.

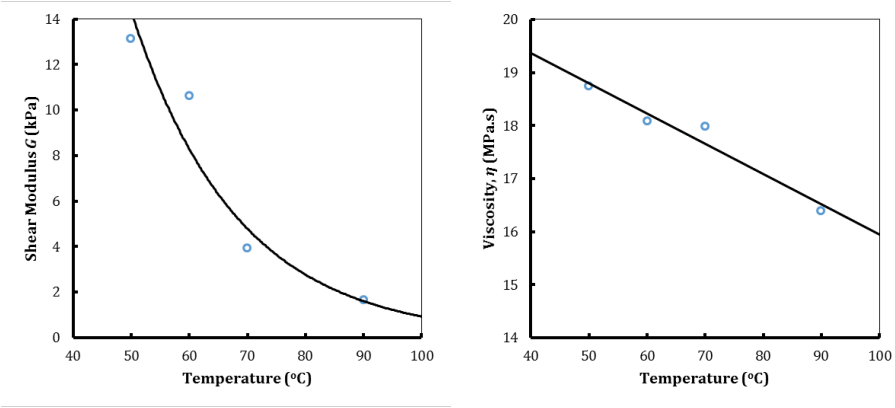

Figure 9: (Left) Rate independent shear modulus G against temperature. (Right) Coefficient of viscosity η against temperature. All tests conducted at a pressure σ_n = 75kPa.

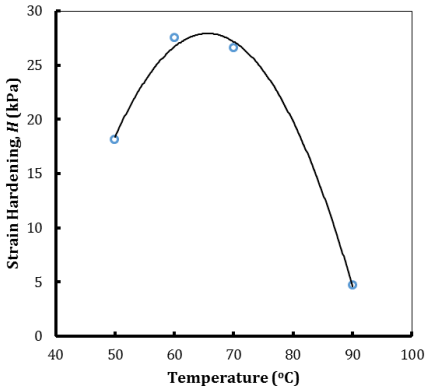

Figure 10: (Left) Strain hardening parameter H against temperature. Test conducted at a pressure σ_n=75kPa

	50°C		**60°C**		**70°C**		**90°C**	
	Value	R^2	Value	R^2	Value	R^2	Value	R^2
G **(kPa)**	13.2	0.981	10.6	0.986	3.93	0.992	1.66	0.973
η **(MPa.s)**	18.7	0.985	18.1	0.986	18.0	0.998	16.4	0.956
H **(kPa)**	18.1	0.948	27.5	0.983	26.6	0.936	4.69	0.996

Table 3: Experimentally derived vales and regression coefficients for G, η and H respectively. Each regression coefficient was drawn from nine data points conducted at a pressure σ_n=75kPa

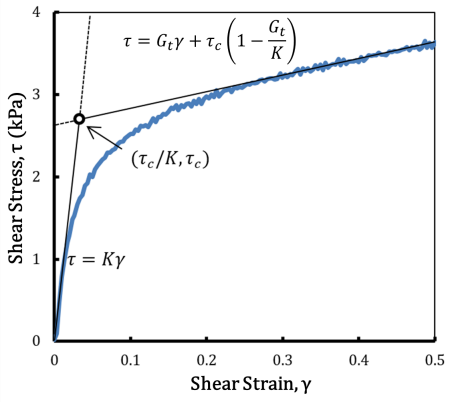

Figure 11: The bi-linear stress-strain response for the viscoelasto-plastic model overlays a typical experimental stress/strain trace for fixed temperature $T = 75°$C, normal pressure $\sigma_n = 75$kPa and strain rate $d\gamma/dt = 3.33\text{e-}3\text{s}^{-1}$. The plot is characterised by two lines, which describe the shear response pre and post-yield ($\tau > \tau_c$).

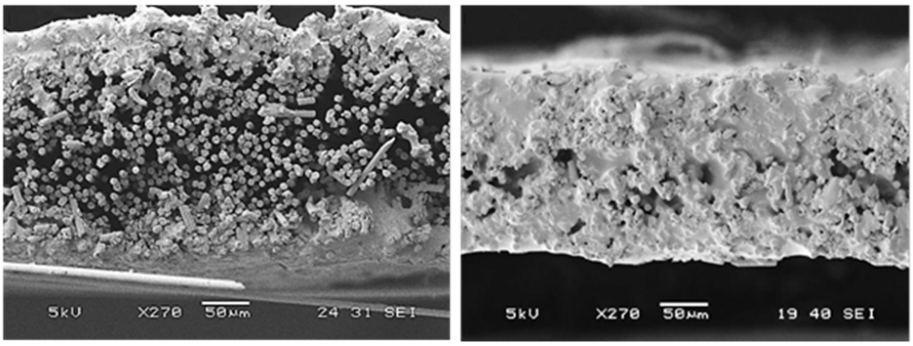

Figure 12: (Left) Cross-section of a single ply of uncured, unconsolidated AS4/8552 prepreg (magnification x270). (Right) Cross-section of AS4/8552 prepreg post consolidation at a temperature of 80°C (magnification x270).

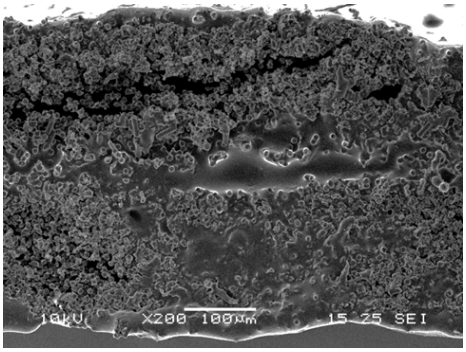

Figure 13: Cross-section of two 0° plies of uncured, unconsolidated AS4/8552 prepreg (magnification x270).

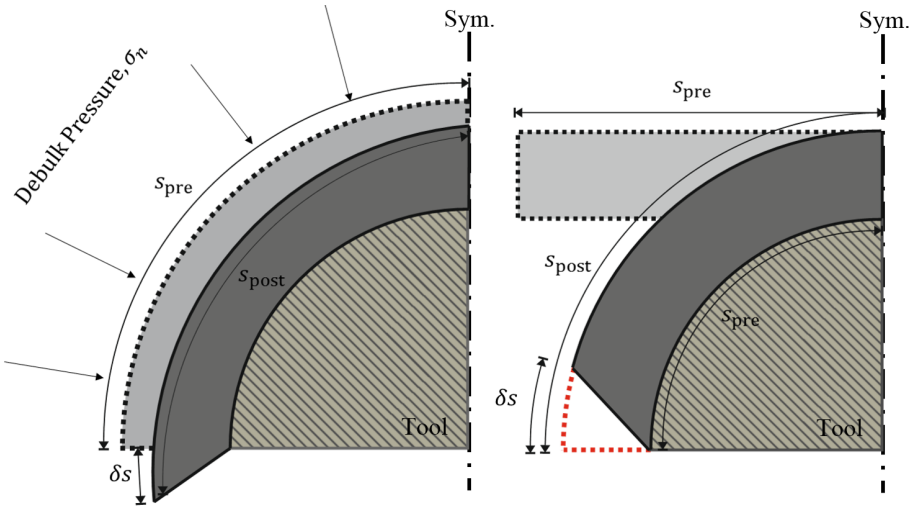

Figure 14: (Left) Consolidation of a composite laminate over one half of a symmetrical semicircular tool. (Right) Drape forming of a composite laminate over the same tool. δs is the total slip. Due to symmetry the right hand edge of the laminate is effectively fixed horizontally.